The Thesis Committee for Aaron Joseph Roberts
Certifies that this is the approved version of the following thesis:

Optical Second Harmonic Generation in Bitumen Films

APPROVED BY
SUPERVISING COMMITTEE:

Supervisor:

Michael C. Downer

Amit Bhasin

Optical Second Harmonic Generation in Bitumen Films

by

Aaron Joseph Roberts, B.A.

Thesis

Presented to the Faculty of the Graduate School of

The University of Texas at Austin

in Partial Fulfillment

of the Requirements

for the Degree of

Master of Arts

The University of Texas at Austin

December 2012

Dedication

Dedicated to my family.

Acknowledgements

I would like to thank Professor Michael Downer for welcoming me to his group and supervising this thesis. His commitment to his students has made my experience in his group truly enjoyable. In addition, I would like to thank all my lab mates who have shown patience with me and whose expertise was invaluable, namely, Junwei Wei, Ming Lei, and Loukas Loumacos. I would also like to thank Farbod Shafiei and Watson Henderson for all the help they gave me at extremely critical times. My gratitude to them is inexpressible. Thank you to Sharmin Sultana for providing me with the samples used in this experiment, and finally, thank you to Professor Amit Bhasin for his collaboration and for approaching our group with the idea that launched this work.

Financial support was provided by the Robert Welch Foundation Grant F-1038, NSF-DMR-0706227, and, NSF-CMMI-1053925.

Abstract

Optical Second Harmonic Generation in Bitumen Films

Aaron Joseph Roberts, MA

The University of Texas at Austin, 2012

Supervisor: Michael C. Downer

The ability of asphalt binders (bitumen) in road surfaces to self-heal after cracking is important to developing a robust transportation system that can tolerate heavy traffic and varying weather conditions. In order to develop improved binders, there is a need for noninvasive, *in-situ,* interface-specific methods of monitoring the kinetics, physics and chemistry of self-healing bitumen interfaces. Here the feasibility of using optical second-harmonic generation (SHG) by focused femtosecond laser pulses to monitor bitumen surfaces is demonstrated. SHG signals are observed in transmission through a sample composed of bitumen spin-coated onto a borosilicate microscope coverslip. The SHG signals are absent from uncoated coverslips, demonstrating that they originate from the bitumen layer. Further tests demonstrate that the bitumen-air surface makes the dominant contribution to the SHG signal. The SHG signal is observed to decay on a time scale comparable to typical self-healing times because of sample heating by the incident laser irradiation. Methods to control this effect by translating the sample during data

acquisition are developed. Although the present results were obtained with a single incident wavelength (800 nm), they demonstrate the feasibility of probing bitumen interfaces spectroscopically with tunable light sources in order to monitor bond-specific chemical kinetics.

Table of Contents

List of Figures

Chapter 1: Introduction

1.1 BITUMEN

The roads we drive on are composed of a mixture of asphalt binder and an aggregate. The asphalt is the glue or binder that holds together the aggregate particles that comprise the body of the asphalt concrete. The binder is also referred to as bitumen [1]. Generally speaking, bitumens are composed of various complex arrangements of hydrocarbons that make an exact molecular or structural description impossible. This complexity makes it difficult to establish a priori a quantitative rank between different asphalt binders in terms of their various material properties. The property of interest to this thesis is that of self-healing in asphalt binders. Self-healing is the process by which sustained micro-level damage to the binder heals itself. In particular, this micro-damage may consist of cracks induced due to repeated or excessive loading. The healing process has been described for polymers in various papers, including references [2-4]. Although bitumens are not necessarily polymeric in nature, a similar model was applied to asphalt materials by Bhasin in [5]. The process consists of two steps. The first is simply the coming into contact, referred to as wetting, of two distinct binder surfaces. The second, referred to as intrinsic self-healing, consists of a diffusive process in which random fluctuations allow for individual molecules to reorient themselves as well as pass through the boundary between interfaces in order to recombine the two and thus, to heal the

crack. The complexity of this process as well as the material itself results in a current lack of understanding that would allow for properly accounting for self-healing while determining the fatigue lifetime of a given asphalt binder.

Researchers have begun the process of trying to quantify self-healing; a few examples are [6-9]. However, results so far tend to be hard to generalize on – they are very dependent on the particulars of the parameter space of the problem [10]. One way to quantify the rate of intrinsic self-healing is to take the ratio of a chosen, measurable mechanical property for a composite that represents two wetted interfaces to that of the same mechanical property in the undamaged material [5]. As stated before, however, self-healing consists of two processes: the wetting process which results in an instantaneous strength gain, followed by the diffusive process which results in the time-dependent strength gain embodied by the intrinsic healing function. The healing process has therefore been modeled as the convolution of these two effects [5]:

$$R = \int R_h(t-\tau)\frac{d\varphi(\tau)}{d\tau}d\tau \tag{1.1.1}$$

where R_h is the intrinsic healing function and φ is the wetting distribution. Previous work on quantifying self-healing has generally failed to separate these two processes. In order to isolate the intrinsic healing process subsequent to wetting in the above equation, Bommavaram et al. performed an experiment in which, rather than damaging a single sample, two separate sample surfaces are controllably brought into contact, thus

rendering the wetting distribution in Eq. 1.1.1 a delta function and effectively isolating the intrinsic healing function [10].

1.2 SCOPE

This thesis explores the use of even-order nonlinear optical interactions to probe bitumen surfaces and interfaces. In particular, the processes of second harmonic generation (SHG) and sum frequency generation (SFG) will be considered. These processes are mediated by the second order electric susceptibility, a third rank tensor that mathematically requires two incident electric fields to produce the vectorial electric polarization induced by the presence of an electric field. In the dipole approximation, SHG and SFG are forbidden in the bulk of centrosymmetric media due to inversion symmetry: writing $P^{(2)} = \chi^{(2)}E^2$ (where $P^{(n)}, \chi^{(n)}$ denote the nth order polarization and susceptibility) and noting that upon inversion P→-P, E→-E, yielding $-P^{(2)} = \chi^{(2)}E^2$. We can see that the only $\chi^{(2)}$ that satisfies both equalities is $\chi^{(2)} = 0$ [11]. In centrosymmetric media, however, surfaces and interfaces serve to break inversion symmetry and therefore to act as local sources of SHG. Thus, the process of SHG is potentially a uniquely sensitive probe of surfaces and buried interfaces for a given material system.

Bitumen is roughly amorphous on average, and as such, the inversion symmetry that allows for surface sensitivity might be expected to hold on average as well. The original work in this thesis is proof-of-principle in nature and is an effort to induce a

detectable level of SHG from a thin layer of bitumen spin-coated onto a thin borosilicate microscope coverslip. This work focuses primarily on generating a detectable signal at various interfaces (namely, bitumen-glass, bitumen-air, and bitumen-bitumen) and ultimately demonstrating the feasibility of using these signals to characterize behavioral-structural properties of bitumen interfaces. In particular, we are interested in using molecular level information about bitumen interfaces obtained from nonlinear optical experiments to learn more about the process of and mechanisms by which self-healing of load induced damage occurs in bitumen. Detailed discussion, preliminary results, conclusions, and proposals for future work will follow in Chapter 3.

Chapter 2 will provide a brief introduction to nonlinear optics and present some experimental techniques that are useful in our lab that were anticipated to be required in the experiments with bitumen. The development of these techniques will take place in the context of surface SHG from Si(100) which is an already well-known physical system in terms of its second harmonic response.

Chapter 2: Nonlinear Optics and Applications to Si(100)

2.1 Background on Nonlinear Optics

A nonlinear optical probe shares many of the advantages of a linear optical probe in that it can be non-destructive, non-invasive, and, in many cases, can be applied in-situ. Additionally, optical nonlinearities are highly sensitive to structural anisotropy of the system being probed, to surfaces and interfaces, and to the polarization of the incident fields. Therefore a nonlinear optical response complements a linear optical response. Of course, this extra information can come at its own expense, sometimes embodied in additional experimental difficulties, for example weak signals and the need for expensive, high-intensity lasers, or difficulty of microscopic interpretation. Indeed, many nonlinear optical phenomena lack a firm microscopic theoretical foundation. Many phenomenological, macroscopic descriptions of various nonlinear behaviors accurately predict results, but still fall short of ultimate, first principles, theoretical foundation. References [13-14] are examples of phenomenological treatments for various symmetries and types of samples. References [15-18] use a slightly more physical model in which bonds in a lattice are represented as point-like dipoles interacting with incident fields to calculate nonlinear phenomena, but even these models make several simplifying assumptions.

Despite these difficulties, nonlinear optical probing has recently found its way into a wide array of applications including, but not limited to, imaging of live cells and

other biophysical phenomena [19-20], characterization of chirality [21], pharmaceutical materials [22], and order parameters in liquid crystal systems [23-24], as well as properties of many polymeric physical systems [25-28]. These examples are in addition to the host of success nonlinear optics has enjoyed in metrology of semiconductors. Recently, in our own lab, second harmonic generation has been used to characterize various properties/processes of silicon, including hot carrier injection, size effects and structural properties of silicon nanocrystals, and characterization of step edges on vicinal silicon which is useful knowledge for controlled nanostructure growth [29-33]. Of course these examples are only a small sample of the applications of nonlinear optics. Indeed, several review articles describe additional applications.

2.2 THE NONLINEAR WAVE EQUATION

This section will attempt to mathematically elucidate the origin and nature of some nonlinear optical phenomena. The material response to an incident electromagnetic field can be described by the induced polarization created by the incident field. The polarization acts as a driving term in a wave equation which describes the emission of electromagnetic radiation subsequent to the initial excitation. The induced polarization in the material due to the incident electromagnetic field is mediated by the material's electric susceptibility:

$$P(x,t) = \chi E(x,t) \tag{2.2.1}$$

Traditionally, in the linear approximation, the electric susceptibility, χ, is derived from first principles by modeling the restoration force of an electron excited by incident electromagnetic radiation as a damped, driven oscillator [34]:

$$m(\ddot{x} + \gamma\dot{x} + \omega_0^2 x) = -\mathrm{eE}(x,t), \tag{2.2.2}$$

where m is the electron mass, γ is the damping force, ω_0 is a resonant frequency, -e is the electronic charge, and E is the driving field. Assuming that x and E are proportional $e^{-\mathrm{i}\omega\mathrm{t}}$ [1], the following result is obtained:

$$m(\omega_0^2 - \omega^2 - \mathrm{i}\gamma\omega)x = -\mathrm{eE}(x), \tag{2.2.3}$$

Solving for x in Eq 2.2.3, we arrive at:

$$x = -\frac{\mathrm{eE}(x,t)}{(\omega_0^2 - \omega^2 - \mathrm{i}\gamma\omega)} \tag{2.2.4}$$

Note now that the macroscopic polarization can be written as a sum over each microscopic dipole moment as P = Np=-Nex, where N is the number of oscillators we

[1] Formally since x and E are real quantities, their complex conjugates (c.c.'s), proportional to $e^{\mathrm{i}\omega\mathrm{t}}$, are also present and will lead to terms in x, E, P, and χ analogous to those presented.

sum over (here we assume each oscillator is identical. See Jackson Ch. 7 for the more general case where each oscillator is allowed to have a different strength and resonant frequency). As such, we have:

$$P = \frac{\mathrm{N}\mathrm{e}^2 E(x,t)}{m(\omega_0^2 - \omega^2 - \mathrm{i}\gamma\omega)} \tag{2.2.5}$$

from which we can immediately deduce upon inspection of equation 2.2.1 that:

$$\chi = \frac{\mathrm{N}\mathrm{e}^2}{m(\omega_0^2 - \omega^2 - \mathrm{i}\gamma\omega)} \tag{2.2.6}$$

While this approximation does give useful results, its shortcoming in the high intensity regime is due to the fact that the restoring force is not harmonic, but rather Coulombic, and goes as $1/r^2$. In the wake of the advent of lasers and their introduction into experimental laboratories, the assumption of a harmonic restoring force and thus of linearity in the relationship between the incident field and the induced polarization fails to adequately account for all observable behavior. We can re-derive the general electric susceptibility in terms of the Coulomb potential in order to ascertain mathematically some of the physical behavior the linear susceptibility model does not account for. By a Taylor expansion about the Bohr radius, we can write the following:

$$\frac{-e^2}{r^2} = \frac{-e^2}{[a_0 + (r - a_0)]^2} = \frac{-e^2}{a_0^2}\left(\frac{1}{[1 - \frac{r - a_0}{a_0}]^2}\right) \tag{2.2.7}$$

$$= \frac{-e^2}{a_0}(1 + 2\frac{r - a_0}{a_0} + 3\frac{(r - a_0)^2}{{a_0}^2} + \cdots) \tag{2.2.8}$$

Letting the quantity $\frac{r-a_0}{a_0}$ be called x, our new equation of motion in the presence of a damping force and driving electric field can be written:

$$m(\ddot{x} + \gamma\dot{x} + \omega_0^2 x + \alpha x^2 + \beta x^3 + \cdots) = -\mathrm{eE}(x, t) \tag{2.2.9}$$

where the constants α and β are parameters known as hyperpolarizabilities of the material system being investigated. At their most general, α and β are third and fourth rank tensors, respectively, which allows for anisotropy in the physical system and coupling between different vector components of motion. In a perturbative limit in which x is expanded in a power series in some perturbation strength, λ, and eE(x,t) is replaced with λeE(x,t), this equation of motion can be solved analytically (See Boyd, Ch. 1) [11]. The solution is a power series expansion of the macroscopic polarization with terms of every order in the field strength E, which, following the logic leading to Eq's 2.2.5 and 2.2.6, allows identification of analogous, higher order susceptibilities. This motivates us to write the polarization induced by the incident field in a power series in E as:

$$P^{\mathrm{NL}} = \chi^{(1)}E + \chi^{(2)}E^2 + \chi^{(3)}E^3 + \cdots \tag{2.2.10}$$

where each $\chi^{(n)}$ is an n+1 order tensor to allow generalizability to multiple field components and to accommodate the geometry of the physical system and experimental set up. We can now examine the wave equation for which this induced polarization becomes the driving term. The following derivation will closely follow Boyd, Ch. 1,2.

In a non-magnetic material devoid of free charge or current we have:

$$\nabla \cdot D = 4\pi P = 0 \tag{2.2.11}$$

$$\nabla \times H = \nabla \times B = \frac{1}{c}\frac{\partial D}{\partial t} \tag{2.2.12}$$

Additionally:

$$D = E + 4\pi\rho \tag{2.2.13}$$

The usual manipulation of Maxwell's equations to derive the wave equation of an electromagnetic field gives:

$$\nabla \times \nabla \times E = -\nabla(\nabla \cdot E) - \nabla^2 E = -\nabla^2 E = -\frac{1}{c}\frac{\partial}{\partial t}(\nabla \times B) = -\frac{1}{c^2}\frac{\partial^2 D}{\partial t^2} \tag{2.2.14}$$

where the intermediate equalities are obtained by invoking Eq's 2.2.11 and 2.2.12, and we have assumed a uniform medium (the gradient of the dielectric function is zero) in setting the divergence of E equal to zero. Inserting Eq 2.2.13 to the final equality in Eq 2.2.14, and moving terms containing E to the LHS of the equation we have:

$$\frac{1}{c^2}\frac{\partial^2 E}{\partial t^2} - \nabla^2 E = -\frac{4\pi}{c^2}\frac{\partial^2 P}{\partial t^2} \tag{2.2.15}$$

We can decompose the displacement current and the polarization into their linear and nonlinear counterparts as:

$$D = D^{(1)} + 4\pi P^{\mathrm{NL}} = E + 4\pi P^{(1)} + 4\pi P^{\mathrm{NL}} \tag{2.2.16}$$

upon which insertion into Eq 2.2.15 yields:

$$\frac{1}{c^2}\frac{\partial^2 E}{\partial t^2} + \frac{4\pi}{c^2}\frac{\partial^2 P^{(1)}}{\partial t^2} - \nabla^2 E = \frac{4\pi}{c^2}\frac{\partial^2 P^{\mathrm{NL}}}{\partial t^2} \tag{2.2.17}$$

Let us now introduce the possibility of multiple frequency components being present:

$$(E, D, P) = \sum_{n=1}^{\infty} (E_n, D_n, P_n) e^{-\mathrm{i}\omega_n t} + c.c \tag{2.2.18}$$

If we neglect dissipation, we can account for each frequency component by writing:

$$D_n^{(1)} = \epsilon^{(1)}(\omega_n)E_n \tag{2.2.19}$$

which gives:

$$\frac{1}{c^2}\frac{\partial^2 D_n^{(1)} e^{-\mathrm{i}\omega_n t}}{\partial t^2} - \nabla^2 E_n e^{-\mathrm{i}\omega_n t} = \frac{4\pi}{c^2}\frac{\partial^2 P_n^{\mathrm{NL}} e^{-\mathrm{i}\omega_n t}}{\partial t^2} \tag{2.2.20}$$

$$\frac{1}{c^2}\frac{\partial^2 \epsilon^{(1)}(\omega_n) E_n e^{-\mathrm{i}\omega_n t}}{\partial t^2} - \nabla^2 E_n e^{-\mathrm{i}\omega_n t} = \frac{4\pi}{c^2}\frac{\partial^2 P_n^{\mathrm{NL}} e^{-\mathrm{i}\omega_n t}}{\partial t^2} \tag{2.2.21}$$

$$\frac{\omega_n^2}{c^2}\epsilon^{(1)}(\omega)E_n - \nabla^2 E_n = \frac{4\pi\omega_0^2}{c^2} P_n^{\mathrm{NL}} \tag{2.2.22}$$

To exemplify mathematically the nature of nonlinear behavior, let us examine the driving term in Eq 2.2.22 as given by Eq 2.2.10. For n=2, $P_2^{\mathrm{NL}} = \chi^{(2)}E^2$. Consider the case when two frequency components are present:

$$E = E_1 e^{-\mathrm{i}\omega_1 t} + c.c. + E_2 e^{-\mathrm{i}\omega_2 t} + c.c. \tag{2.2.22}$$

Then,

$$E^2 = \left(E_1 e^{-\mathrm{i}\omega_1 t} + c.c. + E_2 e^{-\mathrm{i}\omega_2 t} + c.c.\right)^2 \tag{2.2.23}$$

which yields the processes of optical rectification (OR), second harmonic generation (SHG), sum frequency generation (SFG), and difference frequency generation (DFG):

$$P = 2\chi^{(2)}(|E_1|^2 + |E_2|^2) + \quad \text{(OR)}$$

$$\chi^{(2)}({E_1}^2 e^{-\mathrm{i}2\omega_1 t} + c.c. + {E_2}^2 e^{-\mathrm{i}2\omega_2 t} + c.c.) + \quad \text{(SHG)}$$

$$2\chi^{(2)}\left(E_1 E_2 e^{-\mathrm{i}(\omega_1+\omega_2)t} + c.c.\right) + \quad \text{(SFG)}$$

$$\chi^{(2)}\begin{pmatrix} E_1 {E_2}^* e^{-\mathrm{i}(\omega_1-\omega_2)t} + c.c. \\ + E_2 {E_1}^* e^{-\mathrm{i}(\omega_2-\omega_1)t} + c.c. \end{pmatrix} \quad \text{(DFG)}$$

Now we can finally see the nature of the nonlinear optical behavior which is the result of the anharmonic, Coulomb restoring force. The insertion of the Coulomb force into the equation of electronic motion motivated a solution that contains higher order analogs to the linear susceptibility, namely, the nonlinear susceptibilities. These terms can give rise to various frequency components in the polarization, which in turn, drive electromagnetic radiation at that frequency. As it is the case, a linear term is still present - any restoring force can be modeled as harmonic, as long as the excitation is weak compared to the restoration. On physical grounds, we can expect the regime of "strong" excitation to begin when the incident field strength approaches that of the strength of the atomic binding field. It is in this regime that various nonlinear effects can become

observable. The effects mediated by the second order susceptibility as shown above are optical rectification, which is a non-radiative process in which a DC electric field develops in the material, SHG, SFG, and DFG, which are radiative processes by which photons at twice either individual input frequency, and the sum and difference of input frequencies are generated. Two different frequencies were included to illustrate the simplest mathematical case for sum and difference frequency generation, but in general, any number of frequency components can be present. A single frequency only yields SHG, while any number of frequencies could yield any combination of their sums and differences.

It is worth noting that although tensorial notation has been largely brushed aside for simplicity of the derivation and discussion, it is a necessary feature of the higher order susceptibilities to accommodate the possibility of anisotropy in the physical system. As a third rank tensor, the second order susceptibility contains 27 terms, while, for example, the even more burdensome fourth rank tensor, third order susceptibility contains 81 terms. Fortunately symmetry considerations can in many cases greatly reduce the number of unique terms in each of these susceptibilities. This not only simplifies the mathematical description, but also decreases the number of measurements that must be taken in order to fully characterize an unknown physical system.

2.3 SECOND HARMONIC MEASUREMENTS ON SI(100)

We now focus on SHG from a Si(100) surface. The purpose is to discuss experimental techniques applied to an already well-characterized system in order to apply similar, sometimes analogous techniques to bitumen samples. The set up used was designed for second harmonic rotational anisotropy scanning (SH-RAS) measurements. In this experimental geometry, shown in Figure 2.1, the reflected fundamental beam is used for alignment purposes.

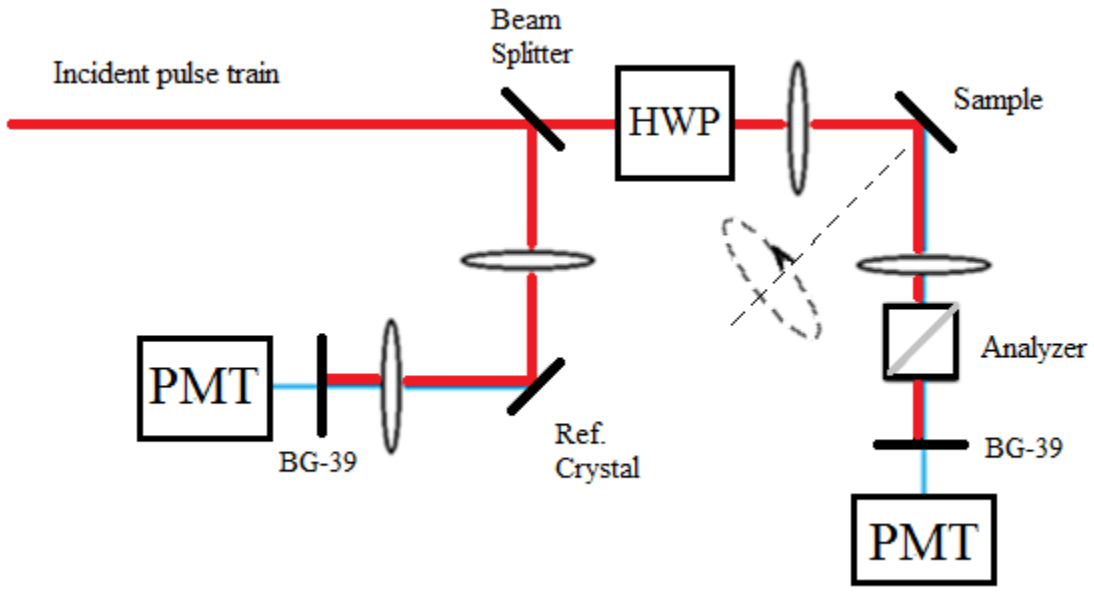

Figure 2.1: SH-RAS experimental geometry

A SH-RAS measurement exploits the fact that the surface of a crystalline material is non-isotropic: the relative orientation of the polarization of the incident excitation and the various bonds that exist at the surface of the material determine the level of second harmonic production at that surface. The measurement is taken by placing the sample at an angle to the incident beam, rotating the sample about the surface normal, and collecting the second harmonic output as a function of azimuthal angle. Because the reflection is not at normal incidence, there is a difference in the signal observed when using incident s or p polarization. Also, due to the tensor nature of the electric susceptibility, either input polarization can, in principle, couple to either output polarization in the SHG process. Therefore, all four unique combinations of p and s input and output polarization configurations can yield a unique signal. The Si(100) surface has an already well-characterized second harmonic response to each of the previously mentioned polarization configurations; $p_{in}p_{out}$ yields a strong second harmonic response, $p_{in}s_{out}$, and $s_{in}p_{out}$ yield intermediate responses, while $s_{in}s_{out}$ yields a very small second harmonic response. In addition, although the response is anisotropic in general, each of these responses can be characterized by their rotational symmetry. Sample data taken from the geometry in Figure 2.1 with each polarization configuration are shown in Figures 2.2-5.

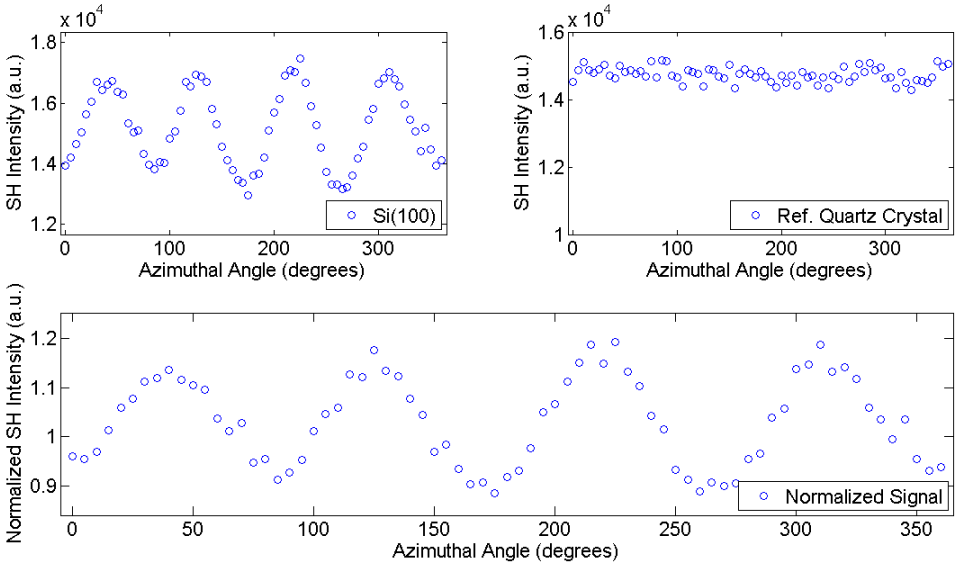

Figure 2.2: $P_{in}P_{out}$ SH-RAS

Upper left) Raw data, upper right) Reference signal, lower) Raw data normalized to reference signal

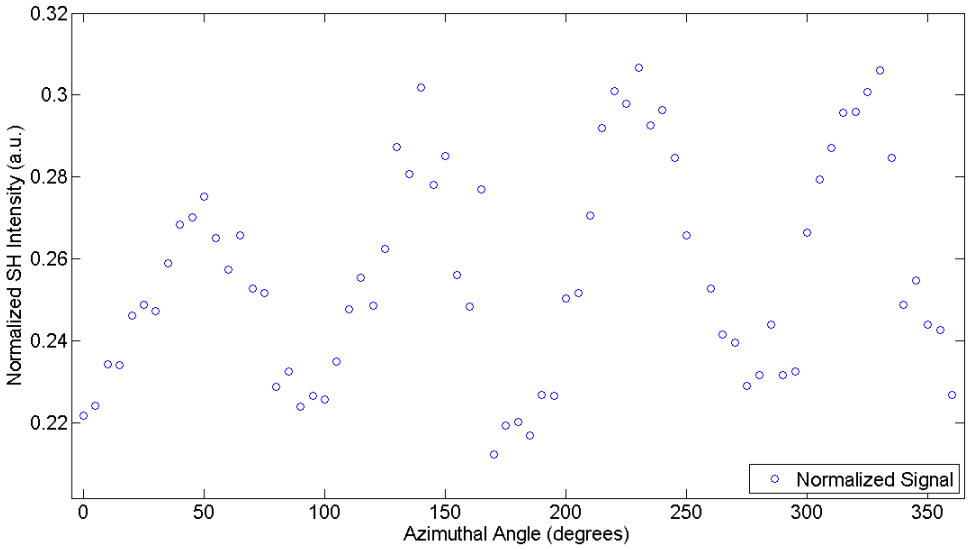

Figure 2.3: $S_{in}P_{out}$ SH-RAS

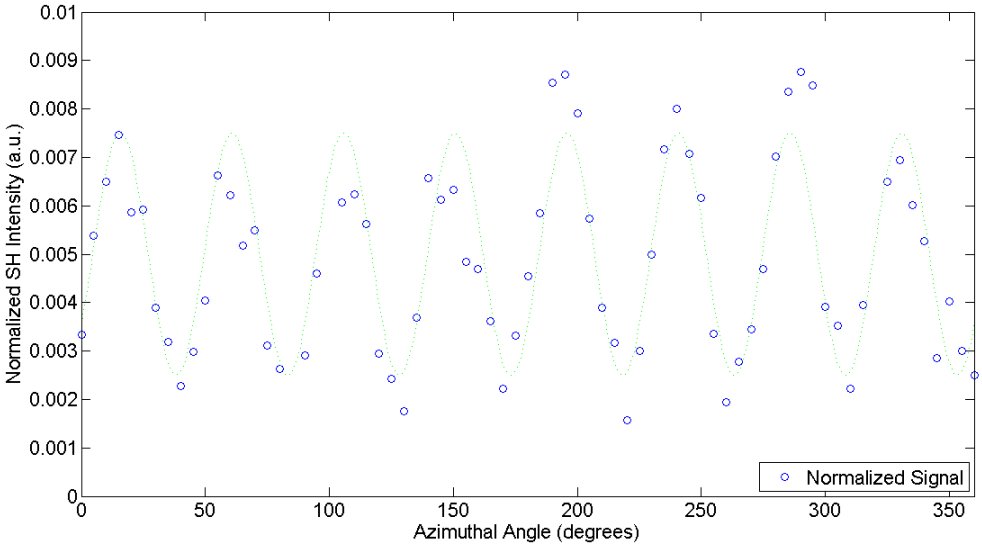

Figure 2.4: $P_{in}S_{out}$ SH-RAS

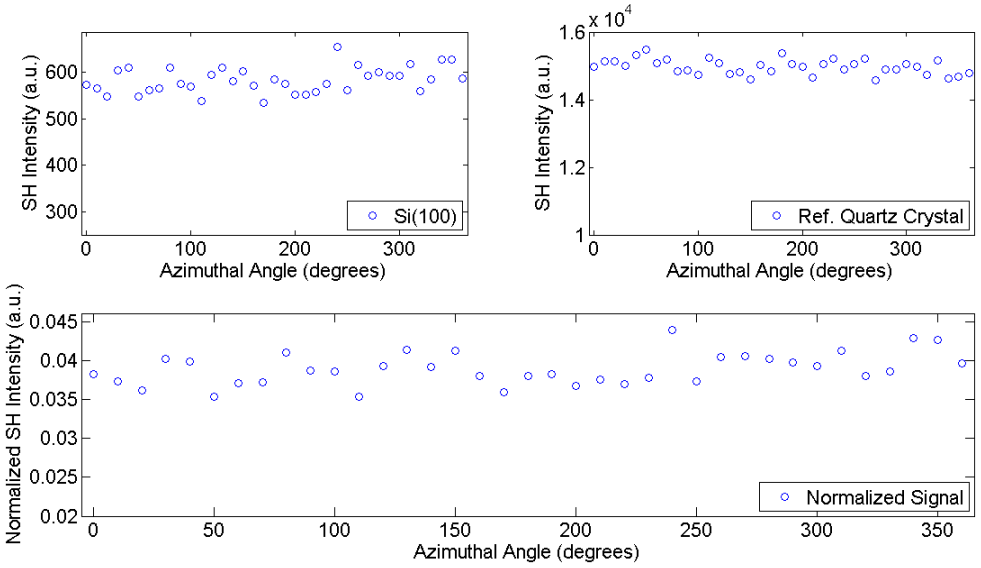

Figure 2.5: $S_{in}S_{out}$ SH-RAS

Upper left) Raw data, upper right) Reference signal, lower) Raw data normalized to reference signal

These measurements were taken using a ~150 fs, ~150 mW, 76MHz rep rate Ti:sapphire laser tuned to a wavelength of 750nm and focused to a ~30μm spot size. It is important to record a reference SH signal from which to normalize the SH signal of interest. In this case, a beam splitter directs some fraction of the incident beam to a quartz crystal from which the reference SH signal is obtained. Normalization to this signal precludes the possibility of changes in SHG levels from being attributable simply to fluctuations in the power output of the laser[2]. In Figures 2.2 and 2.5, all three plots (raw, reference, and normalized) are shown. Figure 2.2 exemplifies how the raw SH signal in the upper left is normalized to the comparably flat signal from the reference quartz crystal in the upper right; the lower area shows a normalized SH response whose variations are independent of laser fluctuations. Figure 2.5 will be discussed shortly.

There are several procedural details that must be observed and are worth noting in this type of experiment. The first step in the RAS process is to ensure that the surface normal is parallel to the axis of rotation. This guarantees that the reflected signal does not wobble laterally about the z-direction while the sample is rotated, which would degrade the integrity of the resulting measurement. The first step in the alignment procedure is to guide the stationary beam through the desired beam path to the detector. Next, the sample is rotated through 360 degrees. Inevitably the beam will be reflected through some kind of closed orbit about its original position. When the rotation is

[2]An additional feature of the SH response of a quartz crystal is that it is spectrally flat in the tunability range of this laser system. The work in this thesis is not spectroscopic in nature, but a spectrally flat reference signal does allow for extension of the techniques outlined to the spectroscopic regime.

finished, the sample surface is re-oriented such that the beam is at the center of the observed orbit. Then the beam is re-aligned to the desired beam path using the subsequent optics. The experimental results are extremely sensitive to this alignment, and thus this process is usually iterated several times in order to obtain the optimal alignment.

After the sample surface normal is aligned to the axis of rotation, it must be ensured that the sample is in the focus of the lens. This is typical of most experiments performed in this lab. In order to accurately place the sample in the focus of the laser, a z-scan is performed, a sample of which is shown in Figure 2.6. A z-scan generally consists of scanning either the focusing optic, or the sample itself in the z-direction. In this case, the lens is scanned. Throughout the scan, the second harmonic output is monitored as a function of the z-position. From the z-scan, the optimal placement of the lens can be determined by finding the z-position corresponding to the highest second harmonic signal.

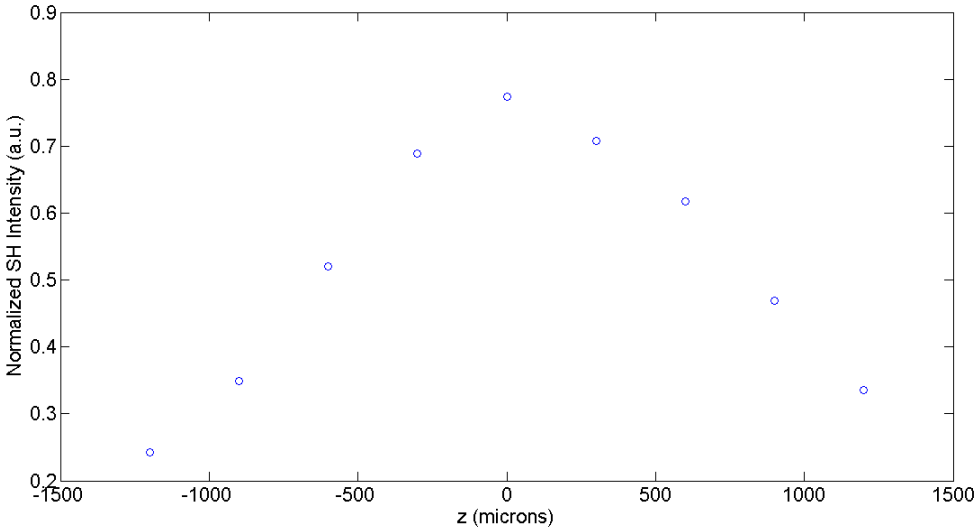

Figure 2.6: A typical z-scan to determine optimal sample placement

The detection method is photon counting via the use of a photomultiplier tube (PMT), a preamplifier, and a photon counter. Another important experimental consideration arises from the fact that the second harmonic output is collimated within the fundamental beam. Some kind of filtering must be performed in order to distinguish between the fundamental and the second harmonic beams. There are several options available. Perhaps the simplest option is spectral filtering through the use of band pass filters. This was the method employed while taking the data presented in Figures 2.2-5. Corning BG-39 filters are often useful in this lab for second harmonic experiments because the fundamental input is frequently near 800 nm and these filters have high transmission in a region including 400 nm, with nearly complete extinction in the region containing 800 nm. Due to the intensity of laser excitation, however, it is possible that

multiple filters must be employed since the transmission of 800 nm light can be non-negligible when the SHG signal is low.

Although measures are already taken to suppress any ambient background light that the PMT might detect such as wrapping the PMT in dark foil and placing it in a sealed enclosure with only a small opening for the signal to enter, a small but nonzero background level is still consistently present even with the laser off or blocked. This count is on the order of ten photons per second for the set up used in this experiment. In addition, while performing the measurements in these geometries, it is inevitable that some stray light from the fundamental will contaminate the signal as well. While the exact background level this amounts to is dependent on the incident power of the fundamental and the reflectivity of the sample, this additional contribution can bring the actual background much higher. In this particular experiment, that number can be on the order of 100 counts. As stated previously, this is important because of the possibility of this background approaching the level of, or even overwhelming the SHG signal. Indeed, in the $s_{in}s_{out}$ configuration no symmetry is evident, and in fact, it appears that the observed signal is entirely due to the leakage of the fundamental. This can be confirmed by watching the signal level change in proportion to adjustments in the incident power despite the fact that we attempt to filter out any remaining fundamental light. Additionally, with a weak signal, there can be diminishing returns to simply using more filters because they are not %100 transmissive either. Fundamental leak through does not play as large a role in the $p_{in}p_{out}$ configuration because the SHG signal is large, and although the $s_{in}p_{out}$ and $p_{in}s_{out}$ signals are smaller, they have the added advantage of

crossed polarizers blocking much of the fundamental and the signals are still large enough that the expected symmetries are evident, which can be regarded as confirmation that the photons being counted are predominantly second harmonic.

For the level of selectivity needed for detection of $s_{in}s_{out}$, the leakage of the fundamental as seen in Figure 2.5 is indeed problematic. In this case it can help to employ a spectrally dispersive device such as a grating, for example, after which the trajectory of each beam diverges. Subsequently the second harmonic beam can be directed to the PMT, while the fundamental beam can be blocked with some opaque obstruction. To this end, a pellin broca prism was employed. The modification to the experimental geometry to include the prism is, in principle, as simple as replacing one of the mirrors in the existing geometry with the prism.

The prism, however, requires a very sensitive alignment and achieves only a small (on the order of 2 degrees) angle of divergence between the fundamental and second harmonic beams. Given adequate table space this is not an intractable problem in and of itself. For example, subsequent to spatial separation the fundamental can simply be guided away from the region of detection or, alternatively, a lens may be used to focus each output beam, with an iris positioned such that only the second harmonic beam passes through its opening. An attempt to use the prism to observe the $s_{in}s_{out}$ signal was made, but this endeavor was hindered by a lack of table space and ultimately the signal was not observed.

2.3 TIME-DEPENDENCE

One last experimental consideration worth discussing is the possibility of time-dependence to the second harmonic signal. In the case of silicon, laser excitation can cause injection of electrons into the charge-carrier region, resulting in the development of an electrostatic field. Continuous exposure to excitation or exposure to high rep-rate (on the order of the life time of the excited state) excitation can thus cause a time-dependent increase in the magnitude of the electrostatic field [35]. This allows for a time-dependent SHG signal mediated by the third order electric susceptibility. Although this is an interesting phenomenon in its own right, it can also convolute in, an unnecessarily burdensome way, an attempt at measuring processes mediated by the second order susceptibility. Figure 2.7 shows the continual rise the SHG signal of a silicon surface irradiated over time with such a high rep-rate laser.

The simplest way to avoid such an effect in practice is to block the beam between measurements. This will work when the time-dependence of an SHG signal is characteristically slower than the time the particular measurement takes. However, this is once again not something that is necessarily known a priori. For an RAS measurement specifically, this effect is largely avoided because the rotation of the sample is usually such that, although the angle of incidence remains constant, the position of the beam on the sample wanders. For other types of measurements the same fortuity is not a guarantee. Time-dependence, albeit of a physically different nature, will become an extremely important experimental consideration in the study of the bitumen samples.

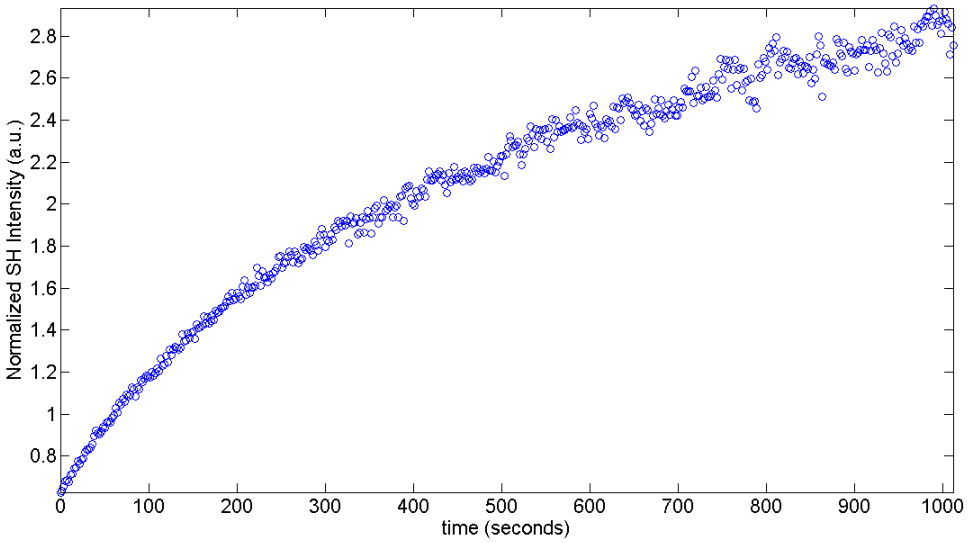

Figure 2.7: Time-dependence of SHG from a silicon surface

Chapter 3: Second Harmonic Generation in Bitumen

3.1 Single Film Bitumen SHG Experiments

The main focus of this thesis is to demonstrate the feasibility of using a second harmonic or sum frequency generation experiment to characterize various bitumen interfaces. Future generations of this experiment will attempt to apply this to characterize self-healing as observed by other methods in [10]. This work presents proof-of-principle second harmonic measurements of bitumen samples where the interfaces present are bitumen-glass, bitumen-air, and bitumen-bitumen.

The samples used are composed of a thin layer of bitumen spin-coated onto a borosilicate microscope coverslip. The samples are examined in the angled transmission geometry shown in Figure 3.1. Initial attempts were made to measure SHG from these samples using the same ~150 fs, ~150 mW, 76MHz rep rate Ti: sapphire laser used to acquire the Si(100) data presented in Chapter 2, however, no signal was observed. A persistent problem at this high repetition rate is cumulative heating of the bitumen film. Because of the low thermal diffusion coefficient of bitumen and the glass substrate, the photo-excited region had no time to cool off between laser pulses. As a result, temperature rose quickly and the film melted, preventing further increases in intensity in an effort to obtain more SHG signal.

To overcome this problem, we switched to an amplified laser system (Positive Light, Inc. Model Spitfire) that provided more energetic (~.1μJ) ~250 fs, 800 nm

wavelength pulses incident upon the sample at only 1kHz repetition rate. In much of the work described below, this pulse train was fed to the sample in bursts of several seconds duration, between which the sample was translated laterally by a distance larger than one focal spot size, in order to inhibit cumulative heating and melting. With this precaution, we found that the beam could be tightly focused to approximately a 5 micron beam waist at 45^{o} incidence angle on the sample surface by a 3cm focal length achromatic doublet, in order to achieve as high an incident intensity as possible. A collecting optic collimates the beam and directs it through an analyzer, Corning BG-39 filters, and into a spectrometer which guides the second harmonic to a PMT. The fundamental is guided with gold mirrors, while the subsequent SHG is guided with aluminum mirrors, a choice guided by the spectral reflectivity of each metal surface. Prior to the focusing optic, a half-wave plate is used so that in combination with the analyzer, we have complete control over which polarization combinations to use. The spectrometer is used to select the wavelength of the light that is directed into the PMT – a grating provides the spatial separation and the placement of a mechanical slit determines the output wavelength. This allows for the clearest possible identification of the SHG without the ambiguity of possible contamination by the fundamental and without having to rely on observation of quadratic power dependence, which is potentially difficult to demonstrate with a low level of signal.

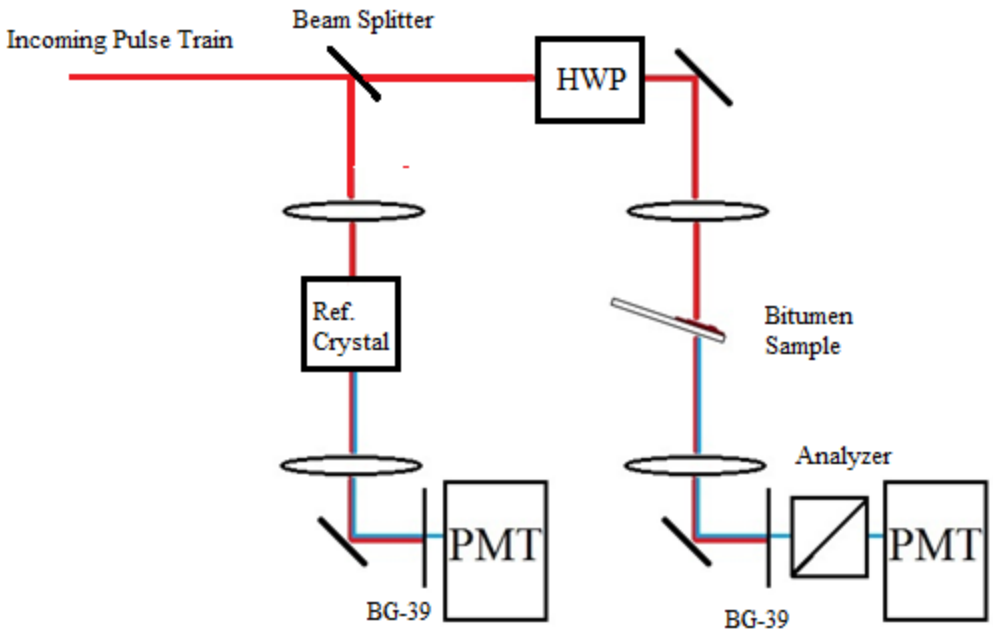

Figure 3.1: Set up for bitumen SHG experiments.

Indeed the first task is to show that we can in fact observe SHG unambiguously. The process of obtaining a spectrum is accomplished by first performing a z-scan of the sample to determine its optimal placement, then varying the position of the slit on the output of the spectrometer to choose the detection wavelength. The z-scans were performed while detecting at 400nm since the incident excitation is 800nm. Initially, it is not known if the detected signal is SHG from the sample or noise at 400nm. This noise could come from various sources in the lab (LEDs on various devices, computer monitors, etc.), or from white light generation within the sample or the optics used. We can preclude the possibility of significant background counts from various lab related light sources by simply counting photons while the input beam is blocked. For our

particular set up this noise source is almost completely extinguished – with the overhead lights off it is easy to reduce the count level to zero when no input beam is present. Additionally, even if the input beam is present without a source of SHG, zero counts can be obtained through a combination of the spatial filtering provided by the monochromater and BG-39's placed before its entrance slit (the filters are necessary).

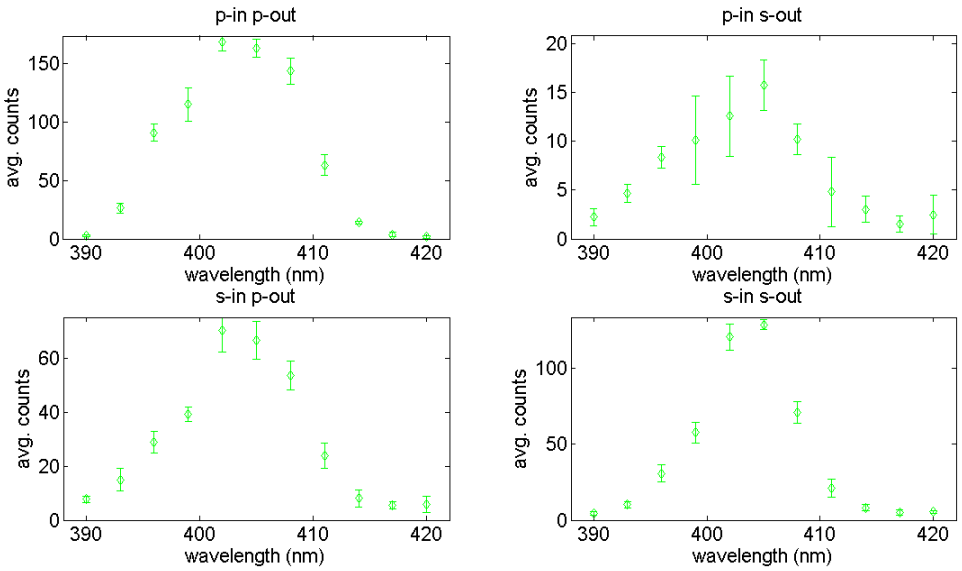

Figure 3.2: Second harmonic spectra in each polarization configuration

It remains to be shown that the photons detected during the z-scan form a peaked spectrum around 400nm as opposed to something that might indicate the presence of a broader white light continuum. Figure 3.2 shows spectra obtained in each of the four polarization configurations. These spectra confirm that the observed signal is second harmonic in nature. Each data point is the average of five counts obtained over a 10

second integration time, with approximately 160μW input laser power. Although this data is not normalized, the raw count levels obtained are typical, making it unlikely that laser fluctuations or background noise were responsible for these peaked spectra.

It further remains to determine that the observed SHG originates from the bitumen as opposed to the glass substrate. The technique employed to this end is to simply translate the sample parallel to its surface until a bare glass area is reached. Figures 3.3-4 show the result of this process for $s_{in}s_{out}$ and $s_{in}p_{out}$ polarization configurations. Again, this data is un-normalized, but it shows the features to be expected if the SHG signals observed in the spectra in Figure 3.2 are indeed attributable to the bitumen. Each of these scans began on the bare glass, and as the sample was translated parallel to its surface a sharp increase in the level of counts is observed corresponding to the position at which the bitumen was first irradiated. The data in Figures 3.2-4 confirm that a second harmonic signal can in fact be observed from our bitumen samples.

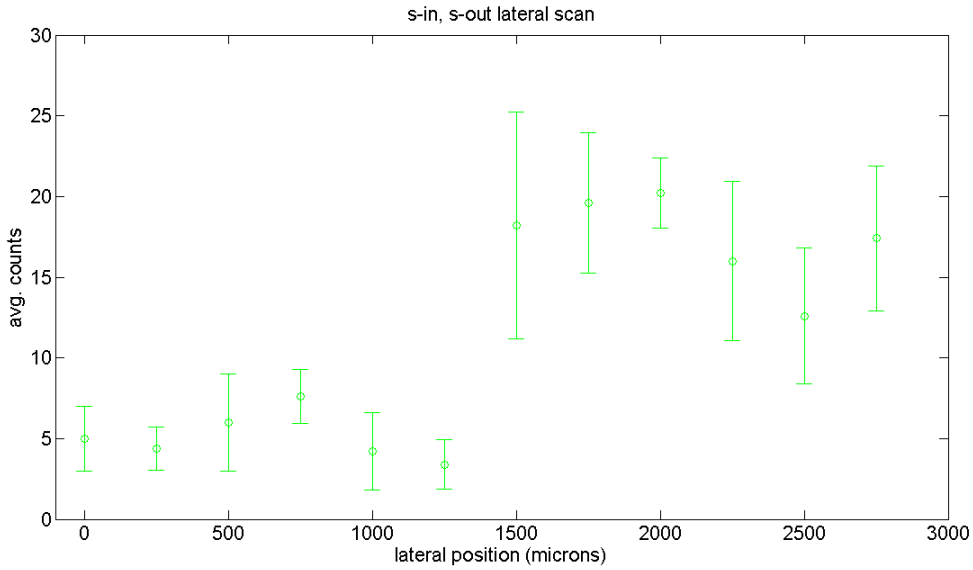

Figure 3.3: Lateral scan from glass substrate (left) to bitumen film (right), ($s_{in}s_{out}$)

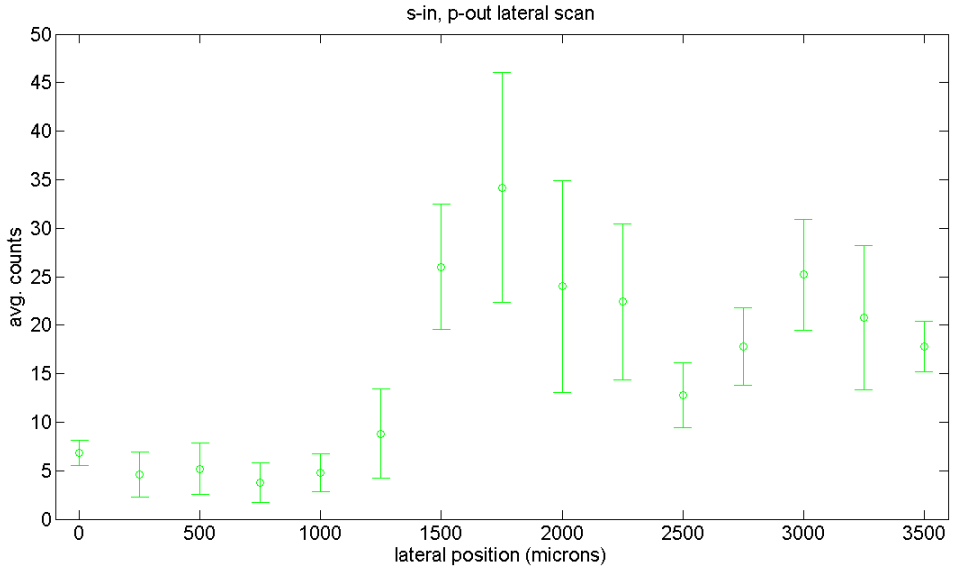

Figure 3.4: Lateral scan from glass substrate (left) to bitumen film (right), ($s_{in}p_{out}$)

3.2 TIME-DEPENDENCE IN SHG FROM SINGLE BITUMEN FILMS

Experimentation subsequent to the data presented in Section 3.1 revealed a time-dependence to the SHG signals that must be addressed. Although it was unknown at the time that data was taken, consideration of the raw count levels in the data in Section 3.1 suggests that the time-dependence did afflict that data. This does not, however, negate the qualitative points shown in that data, namely that a second harmonic signal attributable to the bitumen is observed.

At all intensities which produced observable SHG, a time-dependent decrease in the signal has been observed. This has a very significant impact on the ultimate goal of observing SHG from a system that is evolving in time in order to determine how to use SHG as a probe of the process. As such, the time-dependent decrease from simply leaving the sample under continuous irradiation needs to be resolved. Interestingly, although the signal decays in time, a rest period in which the beam is blocked does illicit some recovery of the signal once the sample is irradiated again. Unfortunately, however, the decay time is on the order of seconds, while the recovery time is on the order of 5-10 minutes. This is problematic because the time scale of the self-healing process is expected to be about an hour. Additionally, this recovery time is not easy to accurately characterize[3] and from sample to sample it is difficult to obtain the level of consistency that would be required in order to confidently use the rest/recovery period to determine

[3] A systematic scan of the length of the rest period was attempted and recovery was quantified by the initial value of the decaying signal after the rest period as a fraction of the initial value of the decaying signal before the rest period, but the resultant determination of a sufficient rest period was not reliable. Moreover, it will be seen later that once a signal which is free from time-dependent decay is obtained, it has a high standard deviation which adds significant uncertainty to the observed recovery anyway.

that any unwanted time-dependence has been removed. Perhaps more importantly, without some conjecture as to the physical changes to the bitumen accompanying both the decay and the recovery of the SHG signal it is impossible to say whether this process would compete with, interfere with, complement, or otherwise affect the natural molecular processes which lead to self-healing in the first place.

Cumulative sample heating, as described earlier, is the most likely cause of the observed time-dependence. There are several options for eliminating this effect. One is simply to reduce the rep rate of the incident fundamental beam. This can be done using a chopper, for example, which simply blocks the beam for an interval of time determined by the desired rep rate before allowing a single pulse and then blocking the beam again. This is not a viable option in our case because we only see approximately one second harmonic photon per 100 pulses. Another possibility is to block the beam between data acquisition periods. The idea here is to record data for a short period of irradiation, rather than allow the irradiation to occur over the time period that would cause the signal to decay to its asymptotic value. This was attempted, and data using various lengths of rest period is presented in Figure 3.6, however, this did not alleviate the problem. Another option available is to record data for a short period of irradiation, block the beam, then to translate the sample laterally in the dark period between data acquisition periods so that a new area of the sample is being irradiated. This ultimately is what was required to obtain a signal free of unwanted time-dependent artifacts.

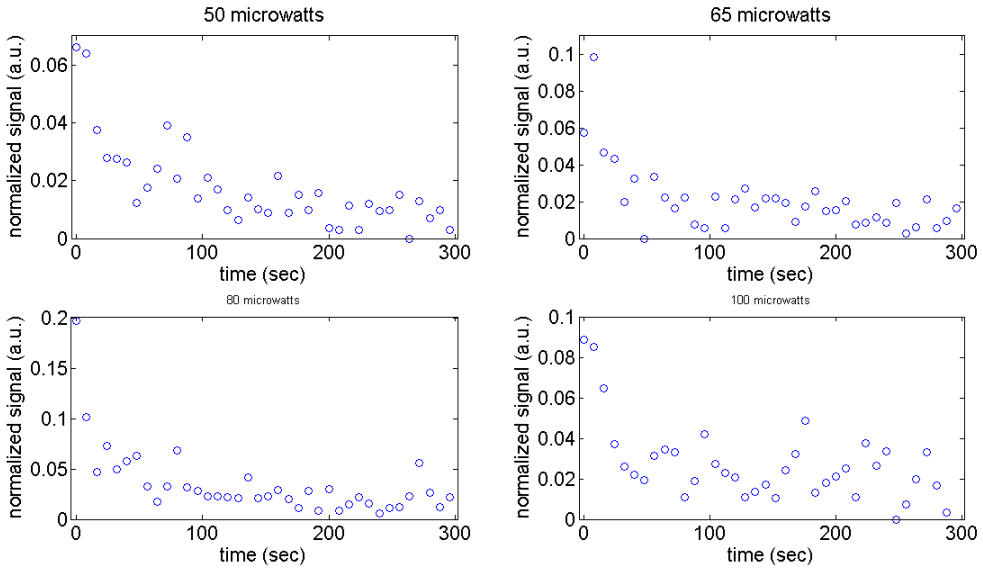

Figure 3.5: Time-dependence of transmitted SHG signal from bitumen film at various average powers, as indicated above each panel, with sample under continuous pulsed fs irradiation at 1 kHz repetition rate.

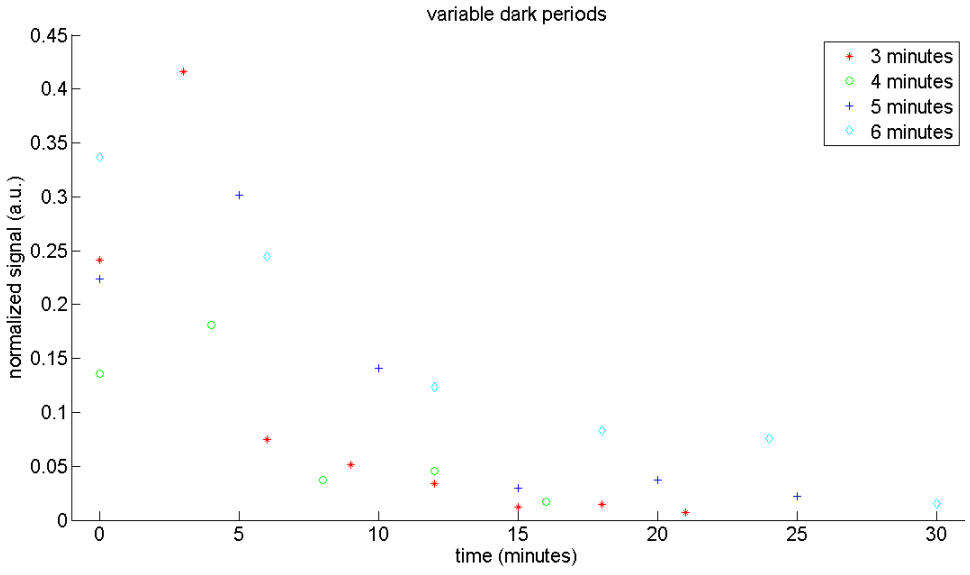

Figure 3.6: Time-dependence of SHG signal from bitumen film with various dark periods, as indicated in the legend, separating fs pulsed irradiation periods of 2 s duration at 1 kHz repetition rate.

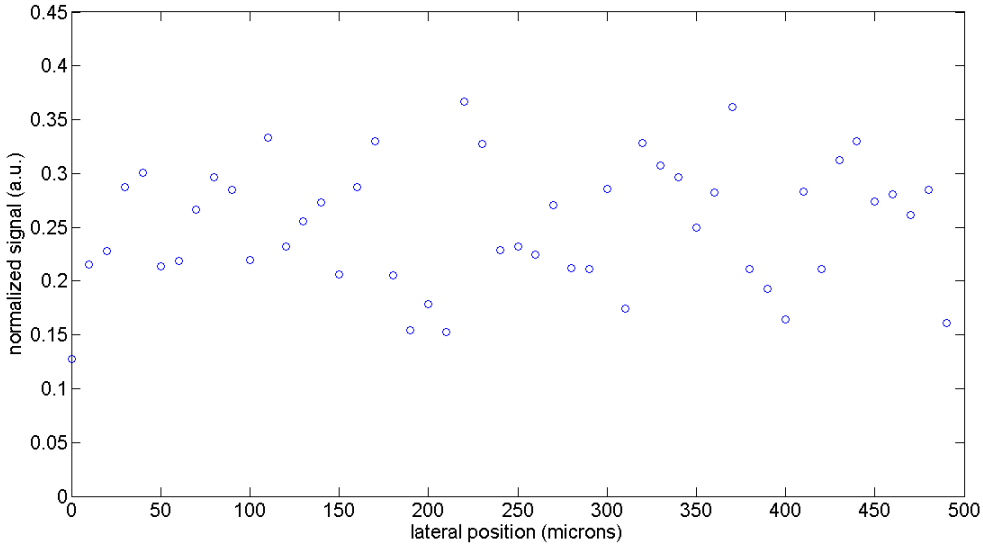

Figure 3.7: SHG signal from bitumen-coated glass slide acquired as in Fig. 3.6, except that the sample was translated laterally by 50 microns during each dark period. Horizontal axis shows translation distance.

The horizontal axis in Figure 3.7 is the lateral position of the scan with respect to its initial position, but there is a correspondence in time. In this data, one minute elapsed between each exposure and the subsequent lateral translation. Each translation was approximately 50 microns. However, there is nothing sacred about one minute or 50 microns. The spot size is only around 5 microns in radius, so theoretically that provides a lower limit to the lateral translation. 50 microns was a safe enough choice to allow for enlargement of the irradiated spot due to imperfect focusing. Parameters such as the translation distance and data acquisition time can be optimized experimentally.

The time between data points should be guided by the number of data points desired in the hour or so in which self-healing is ultimately observed, with this choice

being constrained by the mechanisms used to control the translation. This data was taken by manually blocking the beam and translating the sample each time. Undoubtedly it would be desirable in the future to automate as much of this process as possible. The choice of acquisition time for each data point is a balance between achieving a reasonable raw count level while avoiding over-exposure of the sample in a single data point. In Figure 3.5 a five second integration time was used, while in Figures 3.6-7 a two second integration time was used. The two second integration time achieves a typical raw count level of around 40 counts, consistent with signal level cited earlier of one second harmonic photon per 100 fundamental pulses at 1 kHz rep rate. Two seconds achieved reasonable detail in documenting the signal decay, implying that the signal decayed very little during each individual exposure. Further decrease in the integration time is probably not desirable because the photon count above noise becomes too small. Increasing incident power to compensate runs the risk of increasing sample heating, and accelerating signal decay. Using an amplified kHz laser system that provides shorter pulses (*e.g.* the Femtopower Compact Pro in our group's terawatt lab, which provides 25 fs pulses) of comparable energy, on the other hand, would enable us to apply higher intensity to the bitumen surface, yielding more SHG signal, with less pulse energy and thus less heating.

When translating the sample laterally, the plane of translation must be kept parallel to the sample plane. Any deviations from parallelism could cause the sample to move out of focus, causing a spurious change in second harmonic intensity unrelated to the interface healing dynamics of interest. For a flat sample, this change would be

expected to be monotonic with lateral translation distance. No evidence of such a monotonic change in the signal level exists in Figure 3.7. Figure 3.8 re-enforces this point. Figure 3.8 is a scan from the glass to the sample, again illustrating the desirable contrast between the bare glass and bitumen-covered glass, but also shows that the signal level remains comparable over large lateral distances. Here "large" refers to the total distance potentially translated in the hour or so that self-healing might be observed. Thus, we have achieved the ability to observe a second harmonic signal which is unadulterated by time-dependent decay or any artifacts of the experimental measures employed to suppress it.

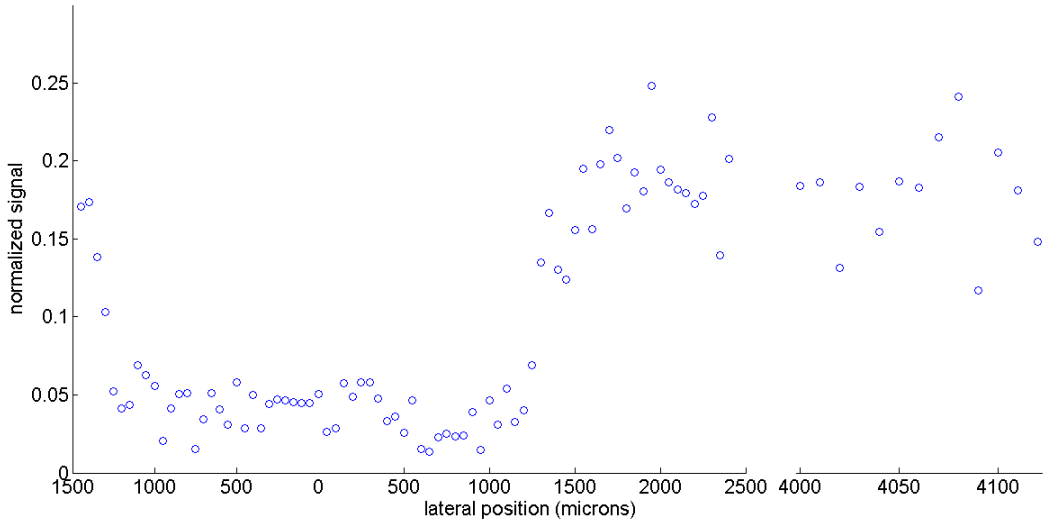

Figure 3.8: Lateral scan from glass substrate (left) to bitumen film (right)

3.3 DETERMINATION OF THE CONTRIBUTING INTERFACES

The last question addressed in this thesis concerns whether the observed second harmonic signal originates from the free bitumen-air surface or the bitumen-glass interface. Centrosymmetry is broken at both of these boundaries, so both are potential sources of dipolar SHG. Moreover, they are separated by only a few microns, and thus are excited simultaneously within the focus of the incident beam, which has a Rayleigh range on the order of a couple hundred microns. In contrast, the glass substrate is 1mm thick, so SHG from the back glass surface can be resolved separately in z-scans. To address this question, we clamped a second microscope cover slip on top of a portion of a bitumen-coated cover slip, creating a region of bitumen in contact with glass at both interfaces alongside a region of bitumen exposed to air. We then scanned the focused laser laterally across the boundary between the two regions while monitoring the SHG signal, using alternating irradiation/dark periods as described in the previous section.

Figure 3.9 shows the result of one such lateral SHG scan. A steady SHG signal, similar in magnitude to the one shown on the right-hand side of Fig. 3.8, is observed from the exposed bitumen film (left). A sharp drop is observed upon crossing the boundary to the glass-covered film (right). This appears to indicate *prima facie* that the bitumen-glass interface contributes minimally to the observed second harmonic signal, and that we can attribute the signal predominately to the exposed bitumen surface. Nevertheless, a possible artifact must be considered. When the focused laser scans onto the glass-covered region, refraction at the top surface of the 1-mm-thick coverslip could displace the focus slightly from the underlying bitumen-glass interface, thereby decreasing the SHG signal simply because of decreased laser intensity at the interface. To check this, we z-scanned both the exposed and glass-covered regions of the sample position through the

incident laser focus. While the exposed bitumen surface yielded a sharp maximum as observed previously, the glass-covered region shows no such peaked feature. The z-scan thus confirms the contrast between exposed and glass-covered bitumen shown in Fig. 3.9. To further confirm this point, a similar lateral SHG scan was performed with the partly exposed/partly covered bitumen film on the back side of the substrate. In this case, the incident laser passes through the same glass substrate in both regions. Data obtained in this manner further confirms the conclusion that the exposed bitumen surface provides the dominant contribution to the observed signal which in turn demonstrates the sensitivity of SHG to the interfacial structure of our bitumen samples.

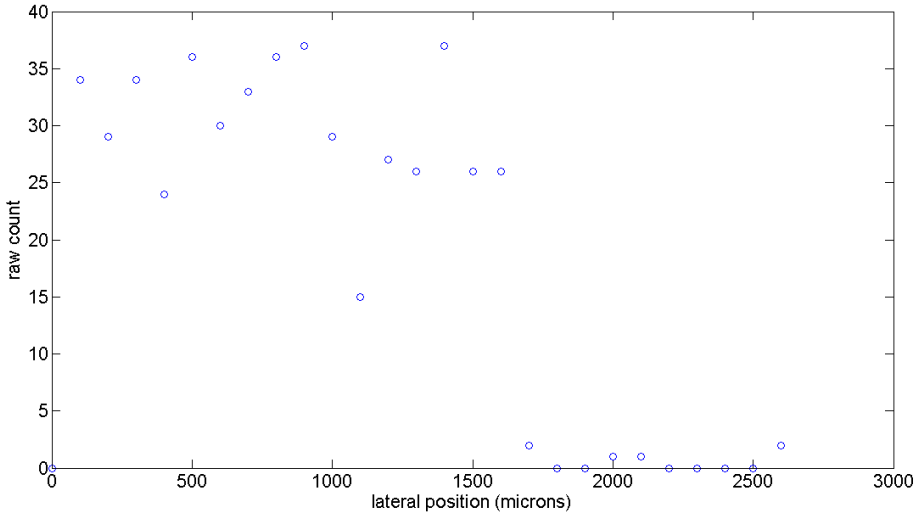

Figure 3.9: Lateral scan of SHG signal from region of exposed bitumen (left) to glass-covered bitumen (right). The boundary between the regions was at approximately 1700 microns on the horizontal scale.

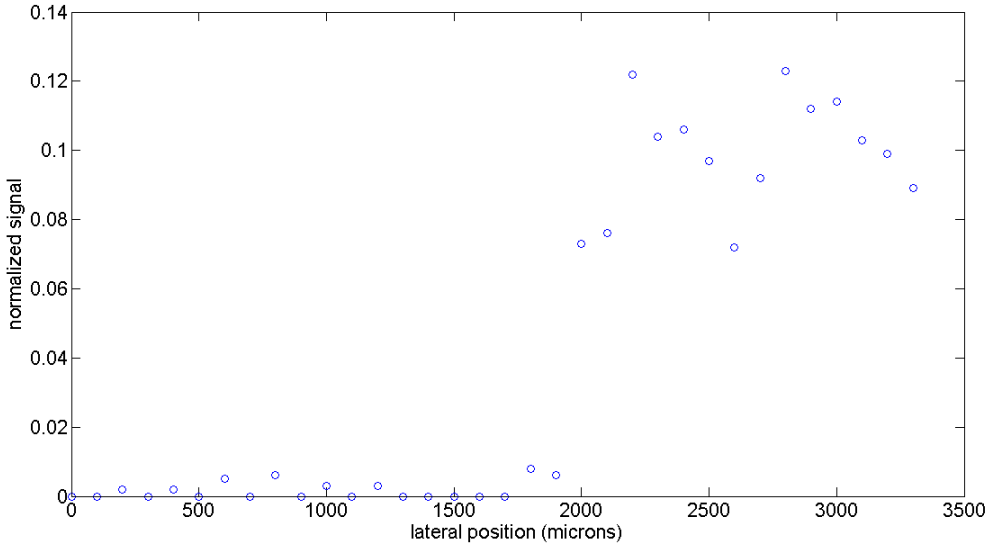

Figure 3.10: Lateral scan from double film region (left) to single film (right) region. The boundary between regions was roughly 2000 microns from the starting position of the scan.

This lateral SHG scan (shown in Figure 3.10) was also performed using a similar sample with the glass-covered region replaced by two bitumen-coated slides, with their bitumen layers in contact, clamped together. After leaving the slides clamped for several days in order to allow the self-healing process to erase the interface between the two samples, a similar sharp decrease in SHG was observed on scanning from the exposed film to the covered region. This implies that SHG should be sensitive to erasure of the interface by self-healing. Attempts have been made to perform this experiment on two samples freshly clamped together. However, they have thus far been unsuccessful due to various experimental difficulties, especially the time required to get the samples into focus in the first place. A credible SHG monitor of the self-healing process is evidently

going to require precise control over the separation of, and compressive force upon, the two free surfaces. These techniques are not yet in hand.

Chapter 4: Conclusions and Future Directions

4.1 Sum Frequency Generation Vibrational Spectroscopy

As indicated in the final equation in chapter one, SHG is only one of several second order nonlinear optical phenomena. It has been demonstrated using SHG that the samples used in our experiments have an accessible surface $\chi^{(2)}$ and that it is sensitive to the nature of the bitumen surface. This has been done at 800 nm excitation. However, the presence of a resonant frequency in Eq 2.2.6 naturally suggests a study which is spectroscopic in nature in order to elucidate any resonances in the material system being probed: when two different frequency components are present, the notation $\chi^{(2)}(\omega_1, \omega_2)$ is usual. Let us denote terms of the functional form

$$\frac{1}{\omega_0^2 - \omega^2 - i\gamma\omega} \tag{4.1.1}$$

as $D(\omega)$. $\chi^{(2)}(\omega_1, \omega_2)$ can be proportional to both $D(\omega_1)$, $D(\omega_2)$, and $D(\omega_{1\pm}\omega_2)$ depending on the particular process being invoked. This implies that the ability to tune either ω_1 or ω_2 makes it possible to discover said resonances in the system and thus to learn more about its structure.

Particularly relevant here is the distinction between using second order nonlinearities as a probe of electronic versus vibrational transitions. As a probe of molecular systems, vibrational transitions are often more useful [36]. In fact, sum-frequency generation vibrational spectroscopy (SFG-VS) has emerged as a powerful technique for determining the surface structure and orientation of polymeric or other macro-molecular systems. Typically this is done using one visible beam and an IR beam where the IR beam can be tuned through a range encompassing various molecular vibrational resonances such as various stretch vibrations. This is an extremely powerful tool for analyzing the presence and orientation of various end groups in macromolecules such as polymers. More relevant to this thesis, however, is the possibility of using the technique to analyze our bitumen samples since it might be expected that a complicated organic molecule as such might contain a rich vibrational structure. In particular, if it can be used to glean information on surface structure at the molecular level, this would be extremely valuable to understanding self-healing in bitumens.

4.2 FUTURE DIRECTIONS

There are many ways this experiment can be improved. The simplest ways generally involve building a set up that is more customized to the needs of this experiment. The most obvious ways involve automation of things such as blocking the beam between data acquisition periods as well as the lateral translations between each data point. This would require some new hardware as well as the development of

LabVIEW VI's to control them. Less trivial than these simple automations would be the development of a sample mount that can hold two samples and control their relative position very precisely. This would ideally allow for the bringing into contact of the two without significantly displacing them in the z-direction so that studies of the self-healing process in time are not limited by the speed at which the samples can be brought into focus after they are brought into contact. In addition, much of the literature about SFG-VS for characterization of complex molecular structures on the surface of materials examines the signal in a reflection geometry. In principle this is an additional experimental adjustment that could be achieved in relatively short order. Apart from mechanical details, it would also be good to develop a set of standard characterization measurements for each sample used. This could address the variability in signal level observed from sample to sample. Improved consistency in this regard would aid in the calculation of absolute values of physical quantities. The least trivial of all the future directions of this experiment is that optical access to vibrational energy levels typically requires IR photons. This means as a probe of vibrational energy structure, a broadly tunable IR source must be developed. An IR optical parametric amplifier (OPA) driven by the same Spitfire Ti:S laser system used for the present research, that produced signal and idler pulses of several micro-Joule energy tunable from 1.1 to 1.9 microns, was in fact designed, built and demonstrated in our laboratory by previous M. S. student Carsten Winterfeldt (M. S. 2002). See Winterfeldt's M. S. dissertation for details [37]. This IR OPA was subsequently converted to a tunable visible (VIS) noncollinear OPA (NOPA) pumped by the second-harmonic of the Spitfire output for optical second-harmonic

spectroscopic studies of silicon nanocrystals. See the dissertation of Junwei Wei (Ph. 2012) for details [38]. Nevertheless, it is possible in principle to reconstitute Winterfeldt's original IR OPA. To generate tunable pulses at vibrational infrared wavelengths (3 to 10 microns), the signal and idler pulses would be mixed in a suitable phase-matched nonlinear crystal to generate their difference frequency. These would then become one of two input pulses in a VIS-IR surface SFG experiment.

Appendix A: Experimental Details

This appendix will describe some experimental details not pertinent to the discussion in the main body of this thesis. It is to provide some guidelines (as opposed to rigid procedures) for conducting experiments on bitumen films.

Alignment of these experiments is typical of any optical experiment. Since the transmission geometry was used, the sample does not actually redirect the beam (appreciably). For this reason alignment is performed without the sample in place. This also removes any issues with exposing the sample continuously to the beam. The two most important aspects of the alignment are ensuring a good focus and good alignment to the entrance slit of the spectrometer used for detection. Because of the general noisiness of the signal, a small focal volume is desired. This minimizes the possibility of signal contamination from second harmonic contributions from anywhere other than the region of interest. A small focal volume is obtained by using a short focal length lens which leads to a small beam waist at focus and a shorter Rayleigh range. Collection of the signal is accomplished by placement of a lens after the focusing optic in order to collimate the signal. It is advantageous to collimate the signal because of the possibility of having to guide it to another area of the table to reach the spectrometer and PMT. Additionally, the signal must be imaged onto the entrance slit of the spectrometer. If the signal is already collimated, a lens can be specifically placed for the purpose of focusing onto the entrance slit of the spectrometer and can be used in other experimental set ups as well without having to be tweaked each time.

Alignment can be performed using either the fundamental or second harmonic generated from a crystal placed where the sample of interest would normally be placed. In practice it is good to check both. To align the image of the beam with the entrance slit the slit is first closed all the way. Typically an IR card can be used to view the image if it is not visible to the naked eye. If the focused beam does not hit the center of the slit, the mirrors prior to the lens can be adjusted to bring the focused beam to the desired position. Once the beam is aligned to the slit, the slit is then re-opened before the experiment is performed. While not in use, it is good practice to block the entrance slit to the spectrometer since it directs light to the PMT. A reference signal is aligned similarly. The reference signal is generated by placing a thin microscope coverslip in the path of the beam. The few percent of reflected light is sufficient to generate the reference signal using a nonlinear crystal. Care must be taken to ensure that this signal does not saturate or damage the PMT it is directed to. While a visible second harmonic signal must be used for alignment, subsequent to this alignment additional filters should be added to attenuate the signal to safe levels for the PMT. The power level typically used in the reference arm is around 30μW (while the sample usually is irradiated by ~μW focused to a beam waist of ~5μm). Additionaly, the orientation of the nonlinear crystal itself can be used to control its second harmonic conversion efficiency.

To minimize noise, gated photon counting is employed. The laser system generates triggers that are receivable by the photon counter. The photon counter then counts only during the allotted gate time. There is an adjustable delay time between when the trigger is received and when counting occurs. This has to manually be adjusted

in order to be sure that the gate time is synchronized to the actual time of arrival of the signal. To make the adjustment, reference second harmonic signals are generated and a scan of the delay time is performed until the optimal delay is determined, as evidenced by a maximal number of counts. This must be performed before beginning any experiment which uses gated photon counting.

Another setting to be determined on the photon counter is the discrimination level. The PMT's send a small current to preamplifiers which convert this signal to a voltage. It is this pulsed voltage that triggers a count in the photon counter. The discrimination level determines the minimum voltage that will register as a count. This level can be determined by examining the output of the preamps with an oscilloscope to see what voltage is characteristic of the pulses. In the experiments done in this thesis, a 200 mV setting was used. While this is something to keep in mind, it is not something that must be done every day.

The experiments were run using the Autocorrelation and CountRecord Labview VI's in the lab. These VI's allow for motor control of sample placement, and manual acquisition of data. The motors translate in finite steps of .625μm. Data acquisition time can be determined by choosing the number of triggers to count over on the photon counter. Z-scans were performed using the Autocorrelation VI which acquires data for the time specified by the photon counter at each point in the z-direction. Typically 50 to 100 steps were taken between points for a rough z-scan used to get close to the focal position and increments of 20 steps were used in z-scans meant for finding the optimal placement in the z-direction. For the lateral scans the sample is brought into focus using

the Autocorrelation VI, then data is counted manually using the CountRecord VI to save the data. For lack of a second programmable motor, the lateral translation was done manually, and CountRecord was used to get a data point at each lateral position. In principle, this process can and should be automated in the future.

Appendix B: Z-scan Artifact and Explanation

Not shown in the data presented of lateral scans between different regions of the samples are the z-scans that were used to place the samples in focus. Figure B.1 is a typical example of such a z-scan. Several features are noteworthy. Two peaks are observed, the first corresponding to the back surface of the glass substrate passing through the focus, the second corresponding to the bitumen covered surface passing through the focus. The width of each peak is consistent with the Rayleigh range of the focused beam.

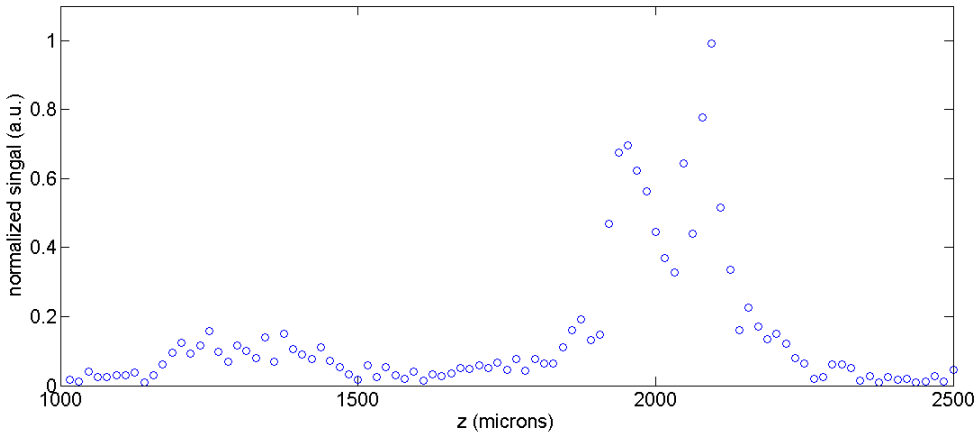

Figure B.1: Z-scan showing peaks corresponding to the back surface of the glass substrate and sample covered surface passing through the focal region

Of more practical implication is the dual-peaked nature of the peak attributed to the bitumen covered surface. Although more systematic investigation would be warranted, it is believed that the nature of this feature is a convolution of the effect of increasing intensity as the sample moves towards the focus and the decay in SHG as the sample is continuously exposed to the incident excitation. The implications are with regard to which z-position is the optimal one to return the sample to prior to lateral scanning. Experimentally it has been observed that subsequent to the z-scan, if the sample is returned to the position of the valley of the two-peaked feature the count level is consistent with the value observed in the z-scan itself. However, if the beam is then blocked, and the sample is translated laterally, the count has been observed to increase to a level similar to that of the shoulders on either side of the valley. Further and more systematic documentation of this particular phenomenon would be valuable.

Bibliography

[1] Hunter, Robert. *Asphalts in Road Construction.* London: Thomas Telford, 2000. Print.

[2] Wool, R. P., and K. M. O'Connor. "Theory of Crack Healing in Polymers."*Journal of Applied Physics* 52.10 (1981): 5933-5963.

[3] Schapery, R. A. "On the mechanics of crack closing and bonding in linear viscoelastic media." *International Journal of Fracture* 39.1 (1989): 163-189.

[4] Kausch, H. H., et al. "Intermolecular interaction in polymer alloys as studied by crack healing." *Polymer Engineering & Science* 27.2 (1987): 149-154.

[5] Bhasin, Amit, et al. "A framework to quantify the effect of healing in bituminous materials using material properties." *Road Materials and Pavement Design*9.sup1 (2008): 219-242.

[6] Kim, Yong-Rak, D. N. Little, and R. L. Lytton. "Fatigue and healing characterization of asphalt mixtures." *Journal of Materials in Civil Engineering*15.1 (2003): 75-83.

[7] Carpenter, Samuel H., and Shihui Shen. "Dissipated energy approach to study hot-mix asphalt healing in fatigue." *Transportation Research Record: Journal of the Transportation Research Board* 1970.-1 (2006): 178-185.

[8] Kim, Booil, and Reynaldo Roque. "Evaluation of healing property of asphalt mixtures." *Transportation Research Record: Journal of the Transportation Research Board* 1970.-1 (2006): 84-91.

[9] Qiu, J., et al. "Investigating the self healing capability of bituminous binders."*Road Materials and Pavement Design* 10.sup1 (2009): 81-94.

[10] Bommavaram, Ramamohan Reddy, Amit Bhasin, and Dallas N. Little. "Determining Intrinsic Healing Properties of Asphalt Binders." *Transportation Research Record: Journal of the Transportation Research Board* 2126.-1 (2009): 47-54.

[11] Boyd, Robert W. *Nonlinear Optics*. San Diego: Academic Press, 1992. Print.

[12] Lüpke, G., D. J. Bottomley, and H. M. Van Driel. "Second-and third-harmonic generation from cubic centrosymmetric crystals with vicinal faces: phenomenological theory and experiment." *JOSA B* 11.1 (1994): 33-44.

[13] Sipe, J. E., D. J. Moss, and H. M. Van Driel. "Phenomenological theory of optical second-and third-harmonic generation from cubic centrosymmetric crystals." *Physical Review B* 35.3 (1987): 1129.

[14] Mizrahi, Victor, and John E. Sipe. "Phenomenological treatment of surface second-harmonic generation." *JOSA B* 5.3 (1988): 660-667.

[15] Powell, G. D., J-F. Wang, and D. E. Aspnes. "Simplified bond-hyperpolarizability model of second harmonic generation." *Physical Review B*65.20 (2002): 205320.

[16] Wang, J-FT, et al. "Simplified bond-hyperpolarizability model of second harmonic generation: Application to Si-dielectric interfaces." *Journal of Vacuum Science & Technology B: Microelectronics and Nanometer Structures* 20.4 (2002): 1699-1705.

[17] Peng, H. J., and D. E. Aspnes. "Calculation of bulk third-harmonic generation from crystalline Si with the simplified bond hyperpolarizability model." *Physical Review B* 70.16 (2004): 165312.

[18] Hansen, J-K., H. J. Peng, and D. E. Aspnes. "Application of the simplified bond-hyperpolarizability model to fourth-harmonic generation." *Journal of Vacuum Science & Technology B: Microelectronics and Nanometer Structures*21.4 (2003): 1798-1803.

[19]Campagnola, Paul J., et al. "High-resolution nonlinear optical imaging of live cells by second harmonic generation." *Biophysical journal* 77.6 (1999): 3341.

[20] Ben-Oren, Ilan, et al. "Infrared nonlinear optical measurements of membrane potential in photoreceptor cells." *Biophysical journal* 71.3 (1996): 1616-1620.

[21] Haupert, Levi M., and Garth J. Simpson. "Chirality in nonlinear optics." *Annual review of physical chemistry* 60 (2009): 345-365.

[22] Lee, Chris J., et al. "Characterization of the bulk properties of pharmaceutical solids using nonlinear optics-a review." *Journal of pharmacy and pharmacology*59.2 (2010): 241-250.

[23] Srivatsa, S. K., and G. S. Ranganath. "New nonlinear optical processes in liquid crystals." *Optics communications* 180.4 (2000): 349-359.

[24] Khoo, Iam Choon. "Nonlinear optics of liquid crystalline materials." *Physics Reports* 471.5 (2009): 221-267.

[25] Chen, Zhan, Y. R. Shen, and Gabor A. Somorjai. "Studies of polymer surfaces by sum frequency generation vibrational spectroscopy." *Annual review of physical chemistry* 53.1 (2002): 437-465.

[26] Gautam, K. S., et al. "Molecular structure of polystyrene at air/polymer and solid/polymer interfaces." *Physical Review Letters* 85.18 (2000): 3854-3857.

[27] Peremans, A., et al. "Vibrational spectroscopy at interfaces by ir-vis sum-frequency generation using CLIO FEL." *Nuclear Instruments and Methods in Physics Research Section A: Accelerators, Spectrometers, Detectors and Associated Equipment* 375.1-3 (1996): 657-661.

[28] Yeganeh, M. S., et al. "Non-linear optical spectroscopy of interfaces: adsorption sites of a self-assembled alkyl thiol monolayerAu (111)." *Thin solid films* 270.1 (1995): 226-229.

[29] Lei, Ming, J. Price, and M. C. Downer. "Hot carrier injection from nanometer-thick silicon-on-insulator films measured by optical second-harmonic generation." *Applied Physics Letters* 96.24 (2010): 241105-241105.

[30] Lei, Ming, et al. "Spectroscopic evaluation of band alignment of atomic layer deposited BeO on Si (100)." *Applied Physics Letters* 100.12 (2012): 122906-122906.

[31] Wirth, Adrian, et al. "Second-harmonic spectroscopy of Si nanocrystals embedded in silica." *physica status solidi (c)* 5.8 (2008): 2662-2666.

[32] Wei, Junwei, et al. "Second-harmonic and linear optical spectroscopic study of silicon nanocrystals embedded in SiO_2." *Physical Review B* 84.16 (2011): 165316.

[33] Ehlert, Robert, et al. "Optical second-harmonic and reflectance-anisotropy spectroscopy of clean and hydrogen-terminated vicinal Si (001) surfaces."*JOSA B* 27.5 (2010): 981-989.

[34] Jackson, John David. *Classical Electrodynamic*. John Wiley & Sons, Inc, 1999. Print.

[35] Mihaychuk, J. G., et al. "Time-dependent second-harmonic generation from the Si-SiO_2 interface induced by charge transfer." *Optics letters*20.20 (1995): 2063-2065.

[36] Chen, Zhan, Y. R. Shen, and Gabor A. Somorjai. "Studies of polymer surfaces by sum frequency generation vibrational spectroscopy." *Annual review of physical chemistry* 53.1 (2002): 437-465.

[37] Winterfeldt, Carsten. "Optical Parametric Amplifier for Nonlinear Optical Spectroscopy." MA Thesis, University of Texas at Austin, 2002.

[38] Wei, Junwei. "Optical Spectroscopy Study of Silicon Nanocrystals." Dissertation, University of Texas at Austin, 2012.